An Investigation of the Protection Afforded a Spacecraft by a Thin Shield

C. J. MAIDEN* AND A. R. MCMILLAN†
General Motors Corporation, Santa Barbara, Calif.

Results are presented from a theoretical and experimental program to investigate the damage that would be inflicted upon a missile, satellite, or space vehicle by a hypervelocity particle. Most of the work has been directed toward thin shield impacts. The problem is treated theoretically by examining the wave motion in an impacting projectile and shield, and consideration is given to heating effects. Theoretical considerations and experimental results lead to the following conclusions: 1) A thin shield is effective because it fragments and spreads the projectile and shield debris and, at high velocities, may melt or vaporize the fragments. 2) The optimum shield to minimize penetration is the one that melts or vaporizes the majority of debris coming through the shield. The shield thickness required to do this is found to decrease with increasing impact velocity. Total damage is not defined on this basis only, and failure may occur through momentum loading of the shielded structure. 3) Shield parameters such as strength and density, on an equiweight basis, are not important. 4) Hole diameter in a shield is proportional to impact velocity and to shield thickness to the two-thirds power.

Introduction

SEVERAL years ago Whipple[1] proposed that a thin outer shell, spaced at a distance from the main hull of a spacecraft, would provide protection against meteoroids. The present paper presents the results of a study to determine the effectiveness of such a meteoroid bumper.

Our present knowledge of the properties of meteoroids is rather limited.[2] The majority of these particles (90% or more) are considered to be of cometary origin and to have the composition of stone.[3] Estimates of density have ranged from 0.05 to 3.0 g/cm^3.[1, 4, 5] The latest estimate is Whipple's[6] value of 0.44 g/cm^3.

The velocities of meteoroids, relative to earth, range from 11 to 72 km/sec. The lower limit is the velocity a particle would acquire if it started from rest relative to earth and then fell several earth radii to the sensible atmosphere. The upper limit is the maximum relative velocity of a collision between the earth and a body in the solar system. Thus, the relative impact velocities of interest to spacecraft designers range from a few to about 80 km/sec. Unfortunately, hypervelocity accelerators such as the one used in this study are limited to 10 km/sec.[7] Also, for convenience, projectiles of fairly high density have been used throughout the experimental program. Thus, emphasis has been placed on studying the physics of the interaction of a hypervelocity projectile with a shielded structure. In this way, confident extrapolations of the present results to higher impact velocities, and other particle densities, can be made.

Experimental Techniques

All experiments were conducted on the ballistic Range "D" facility at the Defense Research Laboratories of General Motors Corporation. This facility consists of a 5.6-mm light-gas gun, an evacuated flight range 6.1 m long, and an impact chamber. The velocity and condition of the model are obtained from spark-shadowgraph stations, and the impact can be observed with a three-channel flash x-ray unit (flash duration of 0.07 μsec).

Impacts in Unprotected Targets

The effectiveness of a protective shield can be observed by comparing the damage produced in protected and unprotected targets. To make this comparison, tests were conducted using 3.2-mm spheres of aluminum as projectiles and unprotected targets of 2024-T3 and 1100-F aluminum. The depths of penetration produced in these tests are shown in Fig. 1. It can be seen that, even at the highest test velocity, the effect of target strength is important, as the values of the normalized penetration for the two target alloys differ considerably. Also, it can be shown that the empirical relationships of Charters and Summers[8] ($p/d \propto v_0^{2/3}$), Eichelberger and Gehring[9] ($p/d \propto v_0^{2/3}$), and Herrmann and Jones[10] all agree with the experimental data to within a factor of 2. This agreement is not too surprising since these empirical equations were derived by curve fitting to experimental measurements.

Unfortunately the forementioned experimental data are limited to velocities of less than 10 km/sec, so no firm statement can be made concerning depth of penetration at higher velocities. The hydrodynamic treatments of Bjork,[11] Walsh,[12]

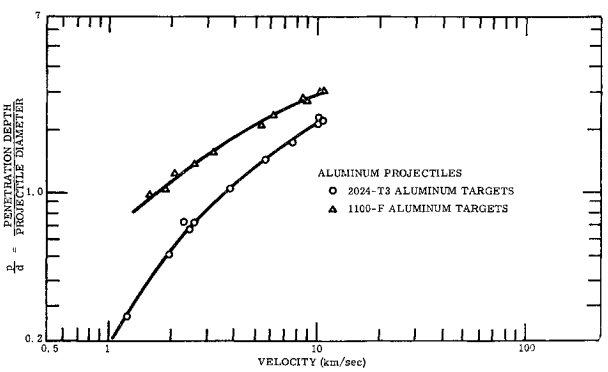

Fig. 1 Comparison of penetration in 2024-T3 and 1100-F aluminum.

Presented as Preprint 64-95 at the AIAA Aerospace Sciences Meeting, New York, January 20–22, 1964; revision received May 28, 1964. This research was supported by the Advanced Research Projects Agency, Ballistic Missile Defense Systems Branch, ARPA Order No. 70, and was monitored by the U. S. Naval Research Laboratory (Code 6240) under Contract No. 3891(00)(X).

* Head, Structural Dynamics Group, Defense Research Laboratories. Member AIAA.

† Senior Research Physicist, High Velocity Impact Group, Defense Research Laboratories. Associate Member AIAA.

and Riney[13] predict that penetration is proportional to $v_0^{1/3}$, $v_0^{0.62}$, and $v_0^{2/3}$, respectively. Bjork ignores strength effects in his analysis, whereas both Walsh and Riney predict that strength and strain rate effects will not disappear with increasing impact velocity. The present experimental results tend to confirm this latter prediction.

Impacts in Protected Targets

Theoretical Model

Consider a right-circular cylinder, whose length is equal to its diameter, impacting a thin shield at hypervelocity. The estimated wave pattern shortly after impact is shown schematically in Fig. 2. It is seen (Fig. 2a) that two shock waves S_1 and S_2 have propagated away from the interface I, and, because the projectile is finite in diameter, rarefaction waves R_1 and R_2 have been transmitted toward the axis of symmetry. Also, the formation of these rarefactions has resulted in the ejection of both projectile and shield material in a rearward direction.

Now consider the situation shortly after the shock S_2 has reflected from the back face of the shield (Fig. 2b). In order to satisfy the boundary condition of zero pressure, the shock is reflected as a rarefaction wave R_3. The resultant particle velocities behind R_3 are such that the profile of the back face of the shield is as shown in the figure. As the process continues, the bubble grows through the addition of material from the shield and projectile.

From a physical viewpoint, the rarefactions R_1, R_2, R_3, and R_4, generated to satisfy boundary conditions, can be looked upon as being tension waves. Hence, fracture will occur if the net tensile stress at any point in the projectile or shield exceeds the fracture stress. In addition, rarefactions will be produced to satisfy boundary conditions at any new fracture surfaces, and these rarefactions can lead to further fractures. Thus, the whole process of fracture of a projectile and a thin shield can be interpreted as a multiple-spalling phenomenon that starts at the free surfaces. Hence, the significance of a shield is that it can fragment the projectile, spread the fragments radially, and significantly reduce the velocity of many of the fragments below the velocity of the original projectile.

Heating Effects Due to Impact

An examination of Fig. 2 shows that during the impact process each element of the projectile and the shield is first shocked to some pressure and is then brought back to ambient pressure by rarefaction waves. This process is represented on a pressure-volume plot in Fig. 3. Each element of material starts off at some initial density ρ_0 and is then compressed on the Hugoniot (points 1–2) to some pressure P_H by a shock wave. The material is then brought back to ambient conditions adiabatically (points 2–3) by rarefaction waves. The initial shocking process is a nonisentropic one, whereas the release process is isentropic. Thus, the entropy of the material has been increased by the impact process. In other words, the element of material in its final state will be heated. The specific internal energy e_H of the shock-compressed material is equal to the area of the dashed triangle $P_H(V_0 - V_H)/2$ in Fig. 3, whereas the energy that is returned by the material in pressure-volume work on expansion is the area under the adiabat. This latter area is less than the area under the triangle, and the difference between the two areas is proportional to the residual heat left in the element. Shocks of low strength will leave the material heated but in the solid state. As the shock strength is increased, the entropy excess increases rapidly and can lead to melting, heated liquid, vaporization, or super-heated vapor in the final state.

A more complete discussion of this phenomenon has been made by Olshaker and Bjork[14] and McQueen and Marsh.[15]

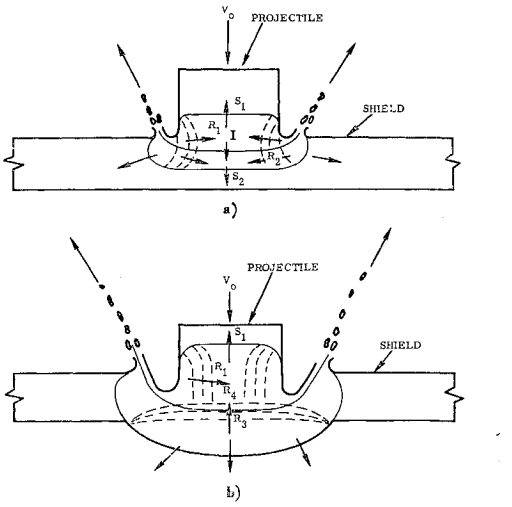

Fig. 2 Estimated wave pattern: a) in a projectile and shield soon after impact; b) after reflection of shock from bottom face of shield.

These workers have calculated, for a number of materials, the values of shock pressure sufficient to cause incipient melting, complete melting, and vaporization when the materials are returned to atmospheric pressure. Some estimated values of these pressures are tabulated in Table 1 for materials of interest in the present paper. Note that, in many cases, appropriate shock pressures for the preceding changes are not available. Also note that the preceding heating effects will be enhanced at low velocities by material viscosity.

It is considered that the forementioned heating effects are important in determining the size of particles in the bubble. If the final debris is in the solid state, the size of spall fragments will decrease with increasing temperature because of a decrease in fracture strength. If the material is molten, only surface tension forces need to be overcome to create droplets; these forces, and hence the droplet size, will become smaller as the liquid becomes hotter. Finally, if the heating effects are great enough, the debris becomes vapor.

Maximum Impact Pressure

The flow between the shocks S_1 and S_2 is one-dimensional until reached by rarefactions R_1 and R_2. The situation in this one-dimensional region immediately after impact is shown in Fig. 4. In this figure, all velocities are measured with respect to a set of coordinates fixed in the shield. The following symbols are used:

v_0 = impact velocity
v_1 = velocity of material between shocks
U_1 = velocity of shock S_1 in projectile
U_2 = velocity of shock S_2 in the shield
P_1 = pressure in region between the shocks

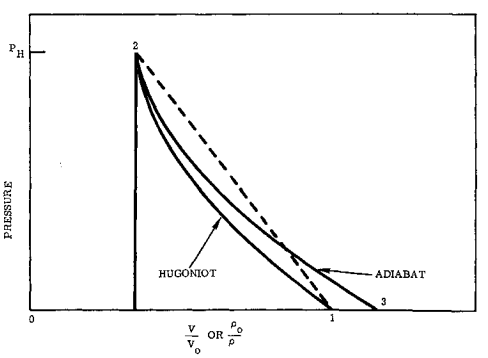

Fig. 3 Pressure-volume curve.

Table 1 Shock heating effects

Material	Melting temperature, °C	Vaporization temperature, °C	Pressure to cause incipient melting Mbar	Pressure to cause complete melting, Mbar	Pressure to cause vaporization, Mbar
Aluminum	660	2057	0.6	0.9	...
Cadmium	321	767	0.4	0.46	0.8
Copper	1083	2336	1.4	>1.8	...
Gold	1063	2600	1.5	1.6	...
Iron	1535	3000	...	2.0	...
Lead	327	1620	0.3	0.35	1.0
Magnesium	651	1107	...	...	...
Nickel	1455	2900	≫1.5	...	...
Titanium	1800	>3000	>1.0	...	...

ρ_0 = density of uncompressed projectile material
ρ_1 = density of projectile material at pressure P_1
q_0 = density of uncompressed shield material
q_1 = density of shield material at pressure P_1

It can be shown that use of the normal-shock relationships across each shock, plus continuity considerations at the interface, produce the following equations:

$$P_1 = \frac{\rho_0 v_0^2}{1 - (\rho_0/\rho_1)}\left[1 + \left(\frac{\rho_0[1 - (q_0/q_1)]}{q_0[1 - (\rho_0/\rho_1)]}\right)^{1/2}\right]^{-2} \quad (1)$$

$$v_1 = v_0\left[1 + \left(\frac{q_0[1 - (\rho_0/\rho_1)]}{\rho_0[1 - (q_0/q_1)]}\right)^{1/2}\right]^{-1} \quad (2)$$

$$U_1 = \frac{v_0 - (\rho_1/\rho_0)v_1}{(\rho_1/\rho_0) - 1} \quad (3)$$

$$U_2 = \frac{v_1}{1 - (q_0/q_1)} \quad (4)$$

In order to solve a specific example, the Hugoniot equations for the projectile and shield materials are necessary. Such equations have been determined experimentally by United States[15, 16] and Soviet scientists[17, 18] for several materials up to 2–5 Mbar. For higher pressures, the theoretical relationships of Walsh and Tillotson[12] may be used.

Effect of Shield Thickness

Figure 2b shows conditions existing after the shock in the shield has reflected as rarefaction wave R_3. The flow in the volume that has not been reached by the rarefactions R_1 and R_2 is one-dimensional and is represented on a time-distance diagram in Fig. 5. The shock S_2 is assumed to reflect from the back of the shield as the centered rarefaction wave R_3. The leading edge of this rarefaction travels at velocity c_{q1} relative to the shield material (moving at velocity v_1) where c_{q1} is the adiabatic speed of sound in the shield material at pressure P_1. Also, reflected and transmitted waves are produced when the rarefaction reaches the interface. The transmitted wave is rarefaction R_4 with the leading edge traveling at velocity $c_{\rho 1}$ relative to the projectile material moving at velocity v_1. Here again, $c_{\rho 1}$ represents the adiabatic speed of sound in the projectile material at pressure P_1. Note that, if the projectile and shield are made of the same material, no reflected wave is produced at the interface.

If the shield is thin enough, rarefaction R_4 can overtake and weaken the shock in the projectile. It can be shown that the leading edge of the rarefaction overtakes the shock at a point in the projectile given by

$$\frac{l}{L} = W\frac{\rho_0}{q_0}\left(\frac{c_{q_1} + U_2 - v_1}{c_{\rho_1} - U_1 - v_1}\right)\left(\frac{c_{\rho_1}}{c_{q_1}}\right)\left(\frac{U_1 + v_0}{U_2}\right) \quad (5)$$

where l is measured from the front face of the uncompressed projectile (length L), t_s is the shield thickness, and W = (weight of shield/unit area)/(weight of projectile/unit area).

In order to calculate l/L from Eq. (5), it is necessary to know the relevant adiabatic speed of sound c_ρ and c_q for each material. If the equations of state of the materials are known, then the speeds of sound can be found from the relationship $c^2 = (\partial P/\partial \rho)_S$, where S denotes differentiation at constant entropy. Unfortunately, even though the Hugoniots of many materials are known, their equations of state are not available. However, the Soviets[19] have measured values of c for several materials and indicate that, for metals up to about 5 Mbar, a reasonable approximation for the adiabatic speed of sound at pressure P behind a shock is given by

$$c_P = D\{0.49 + [(D - v)/D]^2\}^{1/2} \quad (6)$$

where D is the shock velocity relevant to a pressure P, and v is the particle velocity behind the shock. In this equation, both velocities must be measured relative to the undisturbed material considered at rest. Thus, in the coordinates of Fig. 4, $D = U_2$ and $v = v_1$ for the shield material, and $D = U_1 + v_0$ and $v = v_0 - v_1$ for the projectile material.

If, for a specific example, use of Eq. (5) shows that l is less than the length of the projectile L, then the rarefaction R_4 weakens the shock in the projectile. For the impact of like materials and one-dimensional flow, Fowles[20] has pre-

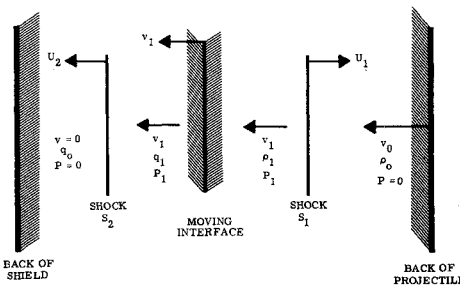

Fig. 4 One-dimensional situation immediately after impact upon shield.

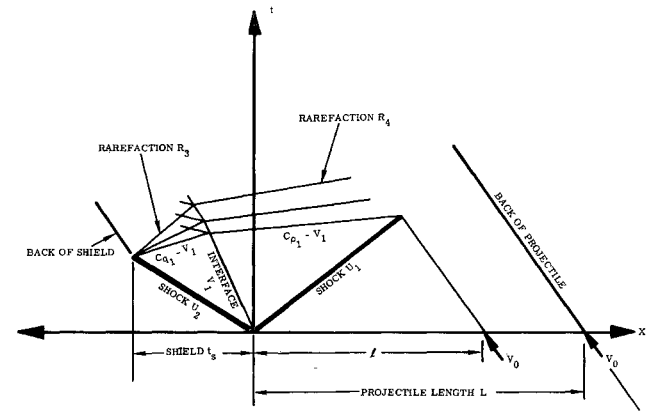

Fig. 5 Time-distance diagram illustrating how the rarefaction from the back of shield overtakes the shock S_1 in a projectile.

sented a method that can be used to calculate how the shock wave S_1 is attenuated by the centered rarefaction wave R_3. In this method, the materials are treated as compressible inviscid fluids, and it is assumed that the entropy is everywhere constant, including across the shock transition. This analysis, on the axis of symmetry, is only valid up until the time the cylindrical rarefaction R_1 (Fig. 2) overtakes the shock S_1 on the axis of symmetry. It can be shown that this occurs at a point in the projectile given by $l_1 = 0.72\ d$, where l_1 is measured from the front face of the initially uncompressed projectile and d is the projectile diameter. For a projectile with $L/d = 1$, it is felt that the error obtained in using the preceding one-dimensional analysis is small.

Impacts in Protected Targets: Experimental Results

Role of Heating Effects Due to Impact

Shield materials of cadmium, copper, and nickel were chosen for these tests, as they have almost identical densities but very different thermal properties. In all cases the protected targets were 6.4-mm aluminum (2024-T3) plates spaced 5.08 cm behind the shields. Also, in all the tests, the shield thickness was kept constant at 1.016 mm.

The first series of tests was conducted using 6.35-mm aluminum spheres at 4.16 km/sec. The targets from these tests are shown in the top rows of Figs. 6a and 6b. It is seen immediately that the frontal damage to the targets decreases in the shield order of nickel, copper, and cadmium. Tables 1 and 2 help explain this result. They show that, at 4.16 km/sec, the maximum impact pressure is only sufficiently high to melt the cadmium debris from the shield, and no melting of copper or nickel fragments will occur. As a result of this, the frontal damage to the backup target with a cadmium shield is reduced significantly. This is because the molten cadmium particles are extremely small, whereas, with the copper and nickel shields, larger solid fragments cause frontal damage to the targets. The x rays from the preceding tests, Fig. 7, show the fragmentary nature of the debris from the nickel and copper shields. Of course, for each test, the debris from the aluminum projectile also causes damage to the backup target; however, the impact pressures for the three shield materials are such that this damage is expected to be least with the nickel, next with the copper, and greatest with cadmium. Thus, the differences in the damage in Fig. 6 are attributable directly to the state of the shield debris.

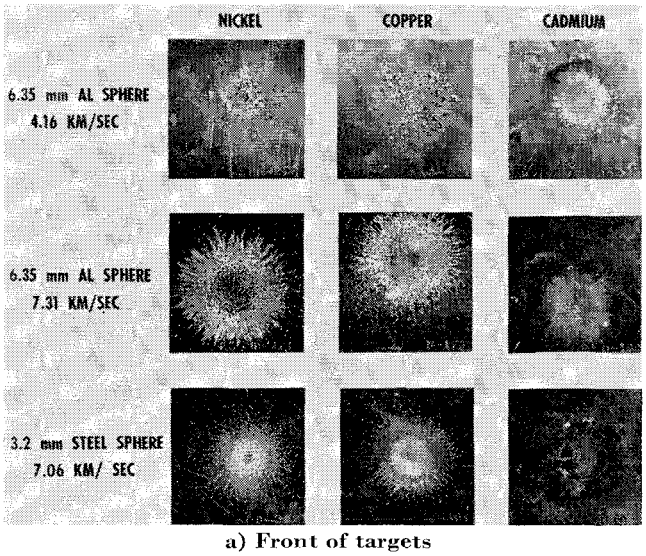

a) Front of targets

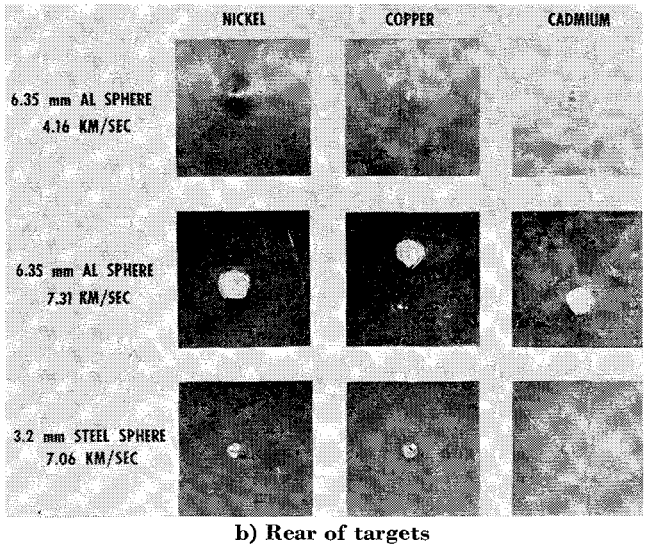

b) Rear of targets

Fig. 6 Effect of shield melting temperature: 1.016-mm shields, 5.08-cm spacing, 6.35-mm 2024-T3 AL backup.

Table 2 Characteristics of impacts in Cd, Cu, and Ni

Projectile	Velocity, km/sec	Shield	Pressure P, Mbar
Aluminum	4.2	Cd	0.67
		Cu	0.72
		Ni	0.75
Aluminum	7.3	Cd	1.50
		Cu	1.57
		Ni	1.67
Steel	7.1	Cd	2.60
		Cu	2.90
		Ni	3.05

In the second series of tests, 6.35-mm aluminum spheres were impacted at 7.31 km/sec. Table 2 shows that the maximum impact pressures generated in these tests are sufficient to cause complete melting of parts of the aluminum projectiles. Also, the pressure is sufficient to vaporize the cadmium and just cause incipient melting of the copper. The targets (second rows of Fig. 6) tend to confirm these theoretical predictions. For instance, a "splash" of aluminum can be observed on all three targets. Also, the frontal damage to the target with a cadmium shield is almost negligible, whereas the presence of pitting on the target with a nickel shield suggests that the nickel fragments are not molten upon impact. Only the x ray for the cadmium shield is shown in Fig. 7 for this series of tests. The x ray definitely confirms that the debris in the bubble exists in other states than solid fragments.

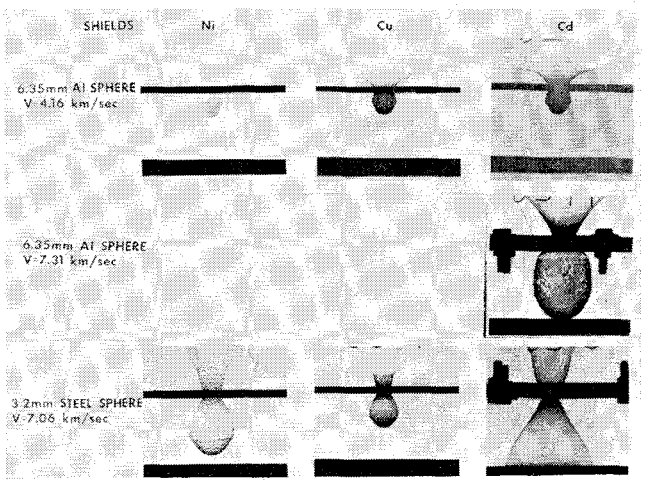

Fig. 7 X rays of impacts against 1.016-mm nickel, copper, and cadmium shields.

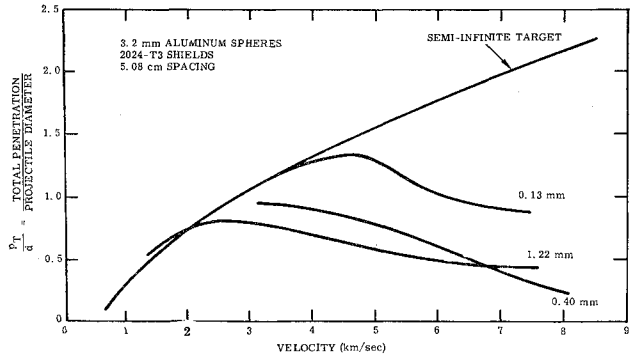

Fig. 8 Total penetration as a function of velocity for aluminum shields of various thicknesses.

The tests in the third series were such that the maximum impact pressure (Table 2) was increased even further than in the first two test series. In these tests, 3.2-mm steel spheres were fired at 7.06 km/sec. The targets are shown in the bottom rows of Fig. 6, and the corresponding x rays are shown in the bottom row of Fig. 7. Once again the cadmium shield is the best; however, now the copper is shocked to a sufficient pressure to become molten, so that the cadmium and copper shields are almost equally effective. Also, both the x ray and target with the nickel shield indicate that the nickel debris is still solid. The x ray for the cadmium shield is such that it is difficult to distinguish any particulate debris in the bubble.

Two points of interest from the foregoing tests should be emphasized. The first point is that both the debris from the projectile and shield cause damage to the backup target. The debris from the shield can be particularly damaging because a large portion of it will travel at near the initial impact velocity. Hence, the state of the debris from the shield is very important in determining the depth of penetration in the backup target. The second point arises from examination of the rear of the backup targets (Fig. 6b). It is seen that the spall-producing load is essentially independent of the state of the material in the bubble.

A Further Comparison of Shield Materials

A further comparison of shields of equal weight, but of different materials, was made at velocities of 4.4, 6.1, and 7.5 km/sec. In these experiments, the projectiles were 4.8-mm aluminum spheres, the main targets were aluminum sheets (2024-T3) 6.4 mm thick, and the separation between shield and target was 5.08 cm in all cases. Tests were conducted at shield weights per unit area of 0.113, 0.226, and 0.452 g/cm², using shields of magnesium (AZ31B-F), aluminum (2024-T3), titanium, copper (OFTP), and gold (24 carat).

The results of the tests indicate the following:

1) To a first approximation, for a given impact velocity, etc., shields of equal weight are approximately equally effective. This suggests that, although the impact pressure P_1 increases as one progresses in density from magnesium to gold shields, the fact that, for such a progression, R_4 catches up with the shock in the projectile more quickly is a compensating factor. In other words, at a given impact velocity, and for shields of equal weight, it would seem likely that the strength of the shock wave S_1 (decayed) that reaches the back of the projectile is similar in all cases.

2) The effects of differences in shield-melting characteristics are not seen as vividly in the forementioned tests as they were for the nickel, copper, and cadmium tests. There are two reasons for this. The first is that the ratios of shield weight per unit area to projectile weight per unit area used in the present tests were less than for the nickel, copper, and cadmium series. Hence, the contribution of the shield to the damage is less. The second reason is that the shield materials used in the present test series do not have as large a spread in melting and vaporization temperatures as nickel, copper, and cadmium.

3) In all the tests, the shield and projectile debris was confined to a conical volume with a semivertex angle of approximately 45°.

Influence of Shield Strength

Several tests were conducted to investigate the effect of shield strength. In all tests, the spacing between shield and backup target was 5.08 cm; also, the backup targets were all 6.4-mm aluminum (2024-T3) plates. Tests were conducted using aluminum and steel shields of various strengths. The aluminum shields were made of 1100-0, 2024-T3, and 7075-T6 aluminum alloys. The steel shields were made of 1020 steel in the as-rolled condition, annealed 4130 steel, and 4130 steel in the normalized condition. Both steel and aluminum projectiles were used in the study.

The general conclusion obtained from all the preceding tests was that shield strength effects are not important. This was expected to be the case at high velocities because of melting of the shield debris; however, apparently the heating effects even at 4 km/sec are sufficient to cause breakup of the shield independent of initial strength characteristics.

Effect of Impact Velocity

The question of how the effectiveness of a shield varies with impact velocity is of particular interest to the spacecraft designer because laboratory test velocities are limited to about 10 km/sec. A series of tests were conducted to shed further light on this problem.

In this series of tests, the projectiles were 3.2-mm aluminum spheres, the spacing between shield and target was 5.08 cm in all cases, and the backup targets were effectively semi-infinite blocks of 2024-T3 aluminum. The tests were conducted over a range of impact velocities. The shields were made of 2024-T3 aluminum, and shield thicknesses of 0.13, 0.40, 0.81, 1.22, and 1.62 mm were used.

The results of some of the tests are shown in Fig. 8 where total depth of penetration p_T (shield thickness plus depth of penetration in the target) has been plotted against impact velocity for shield thicknesses of 0.13, 0.40, and 1.22 mm. Also shown in this figure is the curve for penetration in a semi-infinite target taken from Fig. 1. This latter curve can be looked upon as being the result for a very thick or a negligibly thin shield. With the former, the projectile will not penetrate the shield; with the latter, the shield will be completely ineffective.

The results show that up to about 2 to 4 km/sec the total depth of penetration with a shield is more than the penetration in the unprotected target. Apparently, at these lower velocities, it is easier to perforate the shield than to penetrate

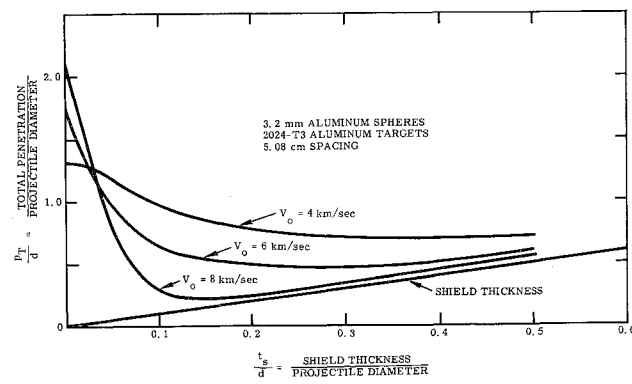

Fig. 9 Total penetration as a function of shield thickness.

an equal distance into a semi-infinite target. However, as the impact velocity is increased, the shields become more and more effective. The reason for this is that fragmentation of the projectile is very small until a velocity of 2.5 to 4.5 km/sec is reached. As the impact velocity is increased above this region, more uniform and complete fragmentation of the projectile occurs. Also, at about 5 km/sec, incipient melting of some of the aluminum debris occurs, and at 6.5 km/sec complete melting of some of the fragments is expected. As a result of this, the curves for the 1.62- and 1.22-mm shields were found to have almost asymptoted to the shield thickness at 8 km/sec. This indicates that the debris impacting the backup target is so small (because of being molten) that it produces negligible penetration. The curves for the other shield thicknesses indicate that, at sufficiently high velocities, they also would asymptote to the shield thickness.

It is of interest to examine how the optimum shield thickness varies with impact velocity. In order to determine this, the total penetration has been plotted as a function of shield thickness at velocities of 4, 6, and 8 km/sec. The results are shown in Fig. 9. Also plotted in this figure is the line corresponding to $p_T = t_s$, i.e., no penetration in the backup target. It is seen that, as the impact velocity increases, the total depth of penetration tends toward the shield thickness at lower values of t_s/d.

These last two facts led the authors to consider the following criterion for selection of an optimum shield. It was postulated that an optimum shield would be of a thickness such that the strength of the axial element of the shock S_1 reaching the back of the projectile would be just of sufficient strength to cause eventual melting of this element. Thus, for aluminum, the maximum shock strength reaching the back of the projectile should be 0.9 Mbar. It was reasoned that, if the shield was any thicker than this optimum value, the axial element of the back of the projectile would still end up in liquid form, only at a higher temperature than the melting temperature. It was felt that in this case the size of the droplets, and hence their damaging ability, would be negligibly smaller than the droplets produced with the optimum shield. On the other hand, if the shield were thinner than the optimum value, the central element of the back of the projectile would remain in the solid state and could cause significant damage.

Based on the foregoing criterion, and using Fowles' solution,[20] the optimum shield thickness for aluminum impacting aluminum was calculated as a function of impact velocity. The results of the calculations are shown in Fig. 10 and clearly show that, based on the present criterion, the optimum shield thickness for minimum total penetration decreases significantly with impact velocity. Also shown in this figure is the experimentally measured optimum at 8 km/sec, and it is seen that the agreement between theory and experiment is good. Unfortunately, melting only occurs at 6.5 km/sec,

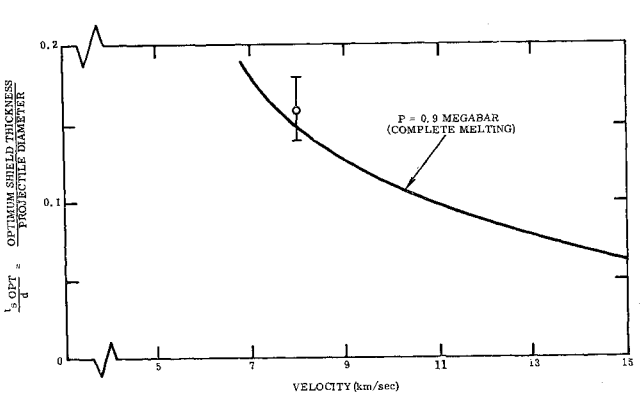

Fig. 10 Calculated optimum shield thickness as a function of impact velocity for aluminum shields and targets.

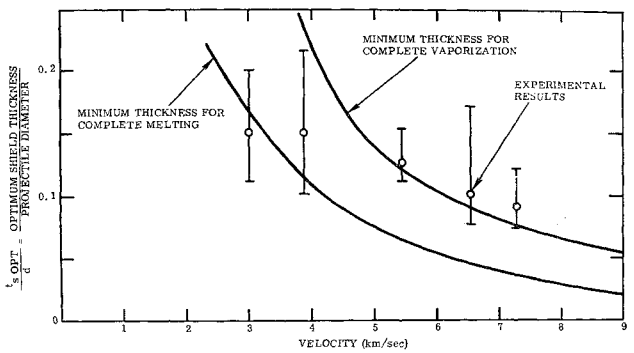

Fig. 11 Calculated optimum shield thickness as a function of impact velocity for cadmium shields and targets.

and the experimental techniques are limited to velocities less than 10 km/sec; thus, the theory is checked only over a limited velocity range.

In order to extend the comparison of theory and experiment over a greater range of velocities, tests were conducted using cadmium projectiles and shields. For such impacts, it was found that melting of some of the debris will occur at about 2.3 km/sec and vaporization at about 3.8 km/sec. Hence, a comparison of the theory with experiment can be made over a greater velocity range than in the aluminum tests.

In these tests the projectiles were 3.2-mm spheres, the backup targets were 6.4-mm-thick aluminum (2024-T3) plates, and the spacing was 5.08 cm. The experiments were conducted at velocities of 3.0, 3.87, 5.44, 6.55, and 7.3 km/sec. The experimental optima from these tests, together with the theoretical optimum shield thicknesses, are shown in Fig. 11. Note that in this figure theoretical curves are shown corresponding to two criteria for selection of an optimum shield. These criteria correspond to conditions where the axial element of the back of the projectile will end up either just molten or just vaporized.

Several comments can be made concerning the results of the preceding tests.

1) Large error bars on the experimental points in Fig. 11 are necessary because the minima of the penetration curves were not clearly defined. Hence, small errors in measurement have considerable influence on the positions of the minima. Despite this, one can draw the following conclusions: At low velocities, there is reasonable agreement between experiment and theory based on the melting criterion. This agreement with the melting criterion at low velocities is not too surprising, because no vaporization occurs at velocities below 3.8 km/sec. At higher velocities it is found that the experimental points agree more with the theory based on the vaporization criterion. It should be noted that the two criteria for selection of an optimum shield are based on the fact that either melting or vaporization of the axial element of the back of the projectile must occur. When either of these conditions are achieved, some material from the sides of the projectile will be in solid form. However, the experimental results indicate that the damaging ability of this debris is small, and that it is not necessary to use a thicker shield than that based on the relevant criterion. This is probably because the debris from the side of the projectile, although not molten or vaporized, is still extremely small. This conclusion is supported by x rays from the tests.

2) It was found that the backup targets corresponding to the 0.20-mm shields ($t_s/d = 0.64$) showed increased damage due to spalling as the impact velocity was increased. This leads to the following important point. The present criterion for selection of an optimum shield only gives the condition for minimum frontal damage ($p_T \rightarrow t_s$) to a backup target. However, the debris impacting such a backup target, even

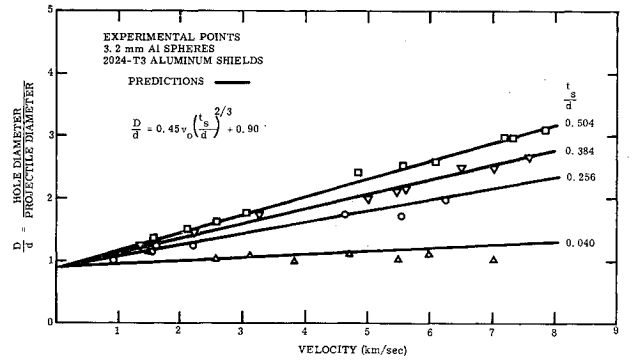

Fig. 12 Hole size in shields for aluminum projectiles and shields.

if in gaseous form, can still exert a severe impulsive loading on the target. This loading can lead to bending of the target, spalling, or the punching out of a segment of the target.

Hole Size in Shield

The hole diameter in the shield was measured in all the experiments performed in the present study. The most revealing results were obtained from the test series on the effects of velocity. The results from this series are shown in Fig. 12. It is seen that, for a specific shield thickness, the hole diameter D is approximately a linear function of velocity. Further investigation reveals that the equation

$$D/d = 0.45v(t_s/d)^{2/3} + 0.90 \qquad (7)$$

where v is impact velocity in kilometers per second, gives a surprisingly good fit to the experimental data, as can be seen in Fig. 12.

It was also found that Eq. (7) is in quite good agreement with the hole size data obtained from the tests using dissimilar shield and projectile materials. These tests indicated [as does Eq. (7)] that hole diameter, at a specific velocity, is fairly independent of shield material and is approximately dependent upon shield thickness alone.

Discussion

The findings of the study to date suggest the following procedure to design a simple spacecraft structure consisting of a meteor bumper and a main hull. Two damage mechanisms must be considered. The first mechanism is complete penetration of the structure by solid particulate debris and is more severe at low impact velocities. This type of damage can be avoided by calculating the optimum bumper for the lowest expected meteoroid velocity. This calculation can be made most easily if the meteoroid and bumper material are assumed the same; hence the properties of the meteoroid have to be estimated. This calculated bumper thickness can then be converted, on an equiweight basis, to the thickness required for any other more suitable bumper material. Such a design procedure will insure that the debris impacting the main hull will be extremely small and will have little penetrating power. At higher impact velocities, this bumper will be even more effective in melting or vaporizing the meteoroid and shield debris.

The second damage mechanism is impulsive failure of the main hull due to the collective impact of the debris that passes through the bumper. This latter type of failure includes both spalling and petalling of the hull and is expected to increase in severity with increasing impact velocity. Thus, the hull must be designed to resist this loading at the greatest expected meteoroid velocity. Both the use of fillers and increased spacing between the bumper and hull will reduce the severity of this type of damage. At the moment, insufficient data are available to estimate (quantitatively) the necessary design requirements to prevent damage by this second mechanism. The present study is continuing in order to shed more light on this aspect of the problem.

References

[1] Whipple, F. L., "The meteoritic risk to space vehicles," *Vistas in Astronautics* (Pergamon Press, New York, 1958), Vol. 2, pp. 115–124.

[2] Maiden, C. J., "Meteoroid impact," *Space Exploration* (Mc Graw-Hill Book Co., Inc. New York, 1964), pp. 236–284.

[3] Whipple, F. L. and Hughes, F. R., "On the velocities and orbits of meteors, fireballs, and meteorites," *Meteors* (Pergamon Press, Ltd., New York, 1955), pp. 149–156.

[4] Whipple, F. L., "A comet model: I—The acceleration of comet Encke," Astrophys. J. **3,** 375 (1950).

[5] Opik, E. J., "Problems in the physics of meteors," Am. J. Phys. **26,** 70 (1958).

[6] Whipple, F. L., "On meteoroids and penetration," J. Geophys. Res. **68,** 4929–4939 (1963).

[7] Curtis, J. S., "An accelerated reservoir light-gas gun," NASA TN D-1144 (1962).

[8] Charters, A. C. and Summers, J. L., "High speed impact of metal projectiles in targets of various materials," *Proceedings of the Third Hypervelocity Impact Symposium* (Armour Research Foundation, Chicago, Ill., 1958), Vol. 2, pp. 101–115.

[9] Eichelberger, R. J. and Gehring, J. W., "Effects of meteoroid impacts on space vehicles," ARS J. **32,** 1583–1591 (1962).

[10] Herrmann, W. and Jones, A. H., "Correlation of hypervelocity impact data," *Proceedings of the Fifth Hypervelocity Impact Symposium* (Colorado School of Mines, Colorado, 1961), Vol. 1, Part 2, pp. 389–438.

[11] Bjork, R. L., "Effect of meteoroid impact on aluminum and steel," Rand Paper P-1662 (1959).

[12] Walsh, J. M. and Tillotson, J. H., "Hydrodynamics of hypervelocity impact," *Proceedings of the Sixth Hypervelocity Impact Symposium* (Firestone Tire and Rubber Co., Akron, Ohio, 1963), Vol. II, pp. 59–104.

[13] Riney, T. D. and Heyda, J. F., "Penetration of structures by hypervelocity projectiles," *Proceedings of the 17th Anti-Missile Research Advisory Committee Meeting* (University of Michigan, Ann Arbor, Mich., 1964).

[14] Olshaker, A. E. and Bjork, R. L., "Hydrodynamics applied to hypervelocity impact—II. The role of melting and vaporization in hypervelocity impact," *Proceedings of the Fifth Hypervelocity Impact Symposium* (Colorado School of Mines, Colorado, 1961), Vol. 1, Part 1, pp. 225–239.

[15] McQueen, R. G. and March, S. P., "Equations of state for nineteen metallic elements from shock wave measurements to two megabars," J. Appl. Phys. **31,** 1253–1269 (1960).

[16] Walsh, J. M., Rice, M. H., McQueen, R. G., and Yarger, F. L., "Shock wave compressions of twenty-seven metals. Equations of state of metals," Phys. Rev. **108,** 196–216 (1957).

[17] Al'Tshuler, L. V., Krupnikov, K. K., and Brazhnik, M. I., "Dynamic compressibility of metals under pressures from 400,000 to 4,000,000 atmospheres," Soviet Phys.—JETP **34,** 614–619 (1958).

[18] Al'Tshuler, L. V., Kormer, S. B., Bakanova, A. A., and Trunin, R. F., "Equation of state for aluminum, copper, and lead in the high pressure region," Soviet Phys.—JETP **11,** 573–579 (1960).

[19] Al'Tshuler, L. V., Kormer, S. B., Brahznik, M. I., Vladimirov, L. A., Speranskaya, M. P., and Funtikov, A. I., "The isentropic compressibility of aluminum, copper, lead, and iron at high pressures," Soviet Phys.—JETP **11,** 766–775 (1960).

[20] Fowles, G. R., "Attenuation of the shock wave produced in a solid by a flying plate," J. Appl. Phys. **31,** 655–661 (1960).